Available online at www.sciencedirect.com
ScienceDirect
Journal of Computational Physics 225 (2007) 2043–2068
JOURNAL OF COMPUTATIONAL PHYSICS
www.elsevier.com/locate/jcp

A mixture formulation for numerical capturing of a two-phase/vapour interface in a porous medium

L.J. Bridge, B.R. Wetton *

Department of Mathematics, University of British Columbia, Vancouver, Canada V6T 1Z2

Received 31 May 2006; received in revised form 5 February 2007; accepted 9 March 2007
Available online 28 March 2007

Abstract

A model problem for two-phase fluid flow and heat transfer with phase change in a porous medium is described. The model is based on a steam–water mixture in sand. Under certain conditions, a two-phase zone, in which liquid and vapour coexist, is separated from a region of only vapour by an interface. A numerical method for locating the interface in the one-dimensional, steady-state problem is described. The results from the steady-state computations are used as benchmarks for the numerical results for the transient problem. It is shown that methods such as front tracking and the level-set method are not practical for the solution of the transient problem, due to the indeterminate nature of the interface velocity, in common with similar degenerate diffusion problems. An interface-capturing method, based on a two-phase mixture formulation, is presented. A finite volume method is developed, and numerical results show evolution to the correct steady state. Furthermore, similarity solutions are found, and the interface is shown to propagate at the correct velocity, by way of a numerical convergence study. Numerical results for the two-dimensional problem are also presented.

Keywords: Two-phase flow; Porous media; Interface capturing

1. Introduction

Two-phase flow and transport in porous media has attracted much interest in recent years, from researchers in such diverse fields as microwave heating of foods and biomaterials [16], geothermal energy recovery [20,26], and fuel cell technology [19,8]. The process of wood drying is examined in detail by Whitaker [25]. Such applications require mathematical models of two-phase flow and phase change which are amenable to numerical solution methods.

The location of interfaces between single-phase and two-phase regions is often of primary interest, and an essential requirement of numerical schemes for the solution of two-phase flow problems is that the interface

* Corresponding author. Tel.: +1 604 822 3784; fax: +1 604 822 6074.
E-mail address: wetton@math.ubc.ca (B.R. Wetton).

0021-9991/$ - see front matter © 2007 Elsevier Inc. All rights reserved.
doi:10.1016/j.jcp.2007.03.011

conditions are accurately satisfied in order for the interface to move with the correct velocity. The model problems we consider in this paper comprise coupled, nonlinear, degenerate parabolic partial differential equations, which have mathematical features in common with Stefan problems, degenerate diffusion, and other free and moving boundary problems.

A popular assumption in the literature is that a region containing two-phase fluid in a porous medium is isothermal, and often a known phase-change temperature is also assumed. Under such assumptions, numerical computations may be greatly simplified. In [4,6], a model problem for one-dimensional, steady-state flow and phase change of water in sand is considered, based on the experimental and analytical work by Udell [21]. In [4,6], a nonisothermal two-phase region model is presented, and it is shown that heat conduction and phase-change effects are greatest near the interface with a liquid-only region. A numerical algorithm is described for computing the location of the free boundaries which separate two-phase region from the regions of vapour and liquid.

The current work concerns methods for capturing the moving interface which separates a vapour/two-phase interface in a porous medium. A natural extension from the steady-state problem to the transient problem results in a ''separate flow model'' [2]. Model problems are formulated in the disjoint domains, which are separated by the moving interface. For moving boundary problems where the interface velocity is readily computed, the disjoint-domain formulation suggests the use of a front-tracking method [7], in which the interface velocity and location are explicitly computed at each time step. Front tracking therefore typically requires a coordinate transformation or re-meshing at each time step. Further, for problems with more than one space dimension, the interface geometry must be considered. The Level Set Method, which also requires an implementation of the interface velocity, has been used for phase change in porous media, in the context of oil reservoir simulation [11]. However, the many simplifying assumptions remove the degeneracy in the problem due to the zero liquid saturation at the interface. In degenerate diffusion problems such as the porous medium equation, the interface velocity is often given by an indeterminate form [17], which makes both front-tracking and Level Set methods impractical.

An alternative to classical front tracking is the Residual Velocity Method proposed for the two-phase Stefan problem in [9]. The idea is to use the front-tracking method, but applied to a steady-state problem, and using the computed residual in one of the interface conditions as an artificial velocity, in order to track the interface to the correct steady state. This method avoids the need for implementing an indeterminate velocity, but it is still essentially a front-tracking method, for which consideration of the interface geometry still presents a significant computational challenge. Also, only the steady-state solutions have any physical meaning.

Fixed-domain, front-capturing methods for the phase change in porous media problem appeal. For the two-phase Stefan problem, the enthalpy method is widely used [1,7]. The problem is reformulated so that a governing equation is valid over the entire domain, containing the interface. The Stefan condition is implicitly absorbed into the formulation, rather than having to be explicitly implemented. This idea has been proposed for phase change in porous media in the fuel cell setting. One method, based on mixture quantities, assumes that the vapour in the two-phase region is at saturation [23]. Another model penalizes any vapour not at saturation pressure into condensing at a large rate [8,19]. Both of these methods require the solution of a fixed-domain problem, from which the interface location can be recovered. Computations are performed under simplifying assumptions of isothermal conditions, and regularisations which smear out the sharp saturation profile.

In this paper, we present a capturing method based on the mixture formulation in [23]. Temperature variation is allowed in the two-phase region. Also, no regularisation is added to the computational problem, and instead we carefully follow the ideas in [10] for conservative schemes for degenerate diffusion problems. A fully implicit, conservative, finite volume scheme is described for capturing the moving interface in the one-dimensional problem. Numerical results show solutions evolving to the correct steady states. Similarity solutions are found for the coupled model problems, and a numerical convergence study shows that the interface moves with the correct velocity. The convergence rates found are comparable with standard capturing methods for prototype scalar problems such as the Stefan problem and the Porous Medium Equation. The method is then extended to higher dimensions.

2. The one-dimensional, steady-state problem

In this section, we describe the steady-state model problem of phase change in a sand pack, as presented by Udell [21]. His experimental results are obtained by partially saturating a sand-filled tube with water, and then heating from the top, while cooling from the bottom, and measuring temperatures along the height of the pack. At steady state, the system supports fluid in the pore space in one of a number of configurations, for example:

(1) Only vapour throughout the entire pack.
(2) A vapour-only zone above a two-phase zone in which both liquid and vapour exist.
(3) A vapour-only zone above a two-phase zone, with a liquid-only zone underneath.

Udell [21] presents experimental results for the three-zone system, where the two-phase zone is identified as the almost isothermal region between two single-phase regions with linear temperature profiles. He then presents an analysis of the two-phase zone only, under the assumption that it is isothermal. We can use Udell's steady-state two-phase zone model as a starting point, which can then be extended to the free interface problem for a two or three-zone system. A disjoint-domain computational method for locating the interfaces in a one-dimensional, steady-state, three-zone (vapour/two-phase/liquid) system is described by Bridge et al [6]. It is worth noting that their model relaxes the popular assumptions of isothermal two-phase zones and phase change only at the boundaries, and we wish to keep temperature and condensation rate effects in this work.

Motivated by the fuel cell setting, where regions of complete liquid water saturation do not occur [3,8,18,19,24], we will concentrate here on a two-zone system which consists of a two-phase zone and a vapour-only zone. We present a computational method, based on that in [6], to compute the interface location in such a steady two-zone system. The numerical results obtained from this method will be used as benchmarks with which we will compare the results from the unsteady computations to be described in later sections.

2.1. Mathematical formulation of the model problem

In Fig. 1, we show a schematic of the basic setup, as used by Udell [21]. The porous layer is initially saturated with a certain amount of liquid water, then heated from above and cooled from below. A steady state is realised, with two distinct zones appearing. In the two-phase zone, $z \in (0, L)$, liquid and vapour coexist in the pore space. In this region, the liquid is driven upward by capillary pressure, while the vapour is driven downward by a vapour pressure gradient. In the vapour-only region, $z \in (L, D)$, the water vapour is stationary. A primary goal of the works by Udell [21] and Bridge et al. [6] is to locate the interface $z = L$. We note that

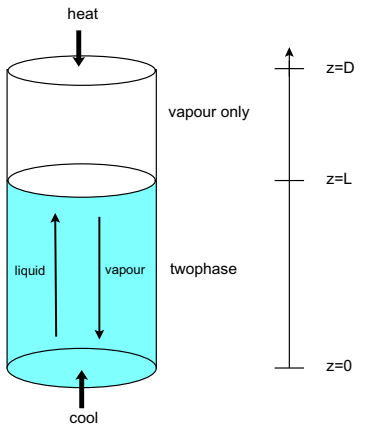

Fig. 1. A two-zone system for Udell's experiment.

the model presented in [6] assumes a constant vapour density throughout the two-phase and vapour-only regions. Here, our model allows for variation in density with temperature, but otherwise, we follow [6]. A list of physical constants and parameters used in our model appears in Table 1.

In order to locate the interface, we consider the saturation s through the porous layer. The saturation is defined by

$$s = \frac{\text{volume of pore space occupied by liquid water}}{\text{volume of pore space}}. \tag{2.1.1}$$

Therefore, a liquid-only region (which we do not consider here) has $s \equiv 1$, a vapour-only region has $s \equiv 0$, and a two-phase region of vapour and liquid has $0 < s < 1$. In this model, we assume that s is continuous throughout the porous layer, and that at the interface $z = L$, we have $s \to 0^+$ as $z \to L^-$. Now, we follow [6] to formulate a model for the saturation s (the liquid volume fraction), and the temperature T, and their variations in z, the height up the porous layer. In the two-phase region $0 < z < L$, conservation of liquid mass gives

$$(\rho_l u_l)_z = \Gamma. \tag{2.1.2}$$

Here, ρ is density, u is the superficial Darcy velocity, Γ is the *condensation rate*, and the subscript l denotes liquid. Conservation of vapour mass is

$$(\rho_v u_v)_z = -\Gamma, \tag{2.1.3}$$

where subscript v now denotes vapour. Conservation of energy is given by

$$0 = (\widehat{K} T_z)_z + h_{\text{vap}} \Gamma, \tag{2.1.4}$$

where $\widehat{K}$ is the effective thermal conductivity of the liquid–vapour saturated porous medium, and h_{vap} is the specific heat of vaporization of water.

The Darcy velocities u_l, u_v are given as follows:

$$u_l = -\frac{\kappa \kappa_{rl}}{\mu_l}((p_l)_z + \rho_l g), \tag{2.1.5}$$

$$u_v = -\frac{\kappa \kappa_{rv}}{\mu_v}(p_z + \rho_v g). \tag{2.1.6}$$

Here, κ is the permeability of the porous medium, p_l is the liquid pressure, p is the vapour pressure, and g is the acceleration due to gravity. The relative permeabilities of liquid and vapour, respectively, are given by

Table 1
Constants for Udell problem

Symbol	Interpretation	Typical value	Units (SI)
ϕ	Porosity	0.38	–
κ	Permeability	6.4×10^{-12}	m^2
ρ_l	Liquid density	10^3	kg/m^3
c_v	Specific heat of vapor	10^3	J/kg K
c_l	Specific heat of liquid water	$4.1 - 4.3 \times 10^3$	J/kg K
μ_v	Viscosity of water vapour	2.2×10^{-5}	kg/m s
μ_l	Viscosity of liquid water	2.5×10^{-4}	kg/m s
$\widehat{K}_v$	Thermal conductivity of vapor saturated medium	1.0	W/m K
$\overline{\rho c}$	Mass averaged density-heat capacity	10^5	J/K m^3
h_{vap}	Latent heat (water liquid–vapor)	2.5×10^6	J/kg
δ	Capillary pressure scaling	1.7642×10^4	Pa
R	Universal gas constant	8.31	J/mol K
M	Molar mass of water	18×10^{-3}	kg/mol
a	Characteristic vapour pressure	0.19743	Pa
b	Characteristic temperature scaling	0.03525	K^{-1}
q	Heat flux	$\sim 10^3$	W/m^2

$$\kappa_{rl} = s^3, \tag{2.1.7}$$

$$\kappa_{rv} = (1-s)^3. \tag{2.1.8}$$

The vapour in the two-phase region is fully saturated, and the temperature and saturation pressure, p_{sat}, approximately obey the exponential relation:

$$p = p_{\text{sat}}(T) = a\,\mathrm{e}^{bT}, \tag{2.1.9}$$

for constants a and b. Next, the capillary pressure, p_{c}, is defined as the difference between the vapour and liquid pressures,

$$p_{\text{c}} = p - p_{\text{l}}. \tag{2.1.10}$$

Now, $p_{\text{c}} = p_{\text{c}}(s)$, the so-called Leverett function [13], and we take

$$p_{\text{c}}(s) = \delta J(s), \tag{2.1.11}$$

where $J(s)$ is given by

$$J(s) = 1.417(1-s) - 2.120(1-s)^2 + 1.263(1-s)^3, \tag{2.1.12}$$

and $\delta = \sigma\left(\frac{\phi}{\kappa}\right)^{\frac{1}{2}}$, where σ is the vapour–liquid interfacial tension, and ϕ is the porosity of the porous medium.

Finally, in the two-phase zone (and indeed throughout the entire system), we assume that the water vapour obeys the ideal gas law, namely

$$p = \frac{R}{M}\rho_{\text{v}} T, \tag{2.1.13}$$

where R and M are the universal gas constant and the molar mass of water, respectively. The work presented by Bridge et al. [6] assumes a constant vapour density, but we wish to include compressibility due to thermal effects here. In summary, the two-phase zone conservation equations (2.1.2)–(2.1.4), together with all the constitutive relations and empirical laws, form a system in three unknowns s, T and Γ. Furthermore, we can eliminate the condensation rate Γ by summing (2.1.2) and (2.1.3), arriving at the system:

$$\left(\frac{\rho_{\text{l}}}{\mu_{\text{l}}} s^3((a\mathrm{e}^{bT} - \delta J(s))_z + \rho_l g) + \frac{\rho_{\text{v}}(T)}{\mu_{\text{v}}}(1-s)^3((a\mathrm{e}^{bT})_z + \rho_{\text{v}}(T)g)\right)_z = 0, \tag{2.1.14}$$

$$\left(\widehat{K} T_z + \frac{\kappa \rho_{\text{v}}(T) h_{\text{vap}}}{\mu_{\text{v}}}(1-s)^3((a\mathrm{e}^{bT})_z + \rho_{\text{v}}(T)g)\right)_z = 0, \tag{2.1.15}$$

together with

$$\rho_{\text{v}}(T) = \left(\frac{Ma}{R}\right)\frac{\mathrm{e}^{bT}}{T}. \tag{2.1.16}$$

Eqs. (2.1.14) and (2.1.15), form a coupled, second-order, nonlinear system for the two-phase zone variables s and T, in the region $0 < z < L$. The system clearly has a singularity and degeneracy at $s = 0$. In the case of constant vapour density, Bridge [4] shows that $s = \mathcal{O}(L-z)^{1/4}$ as $z \to L^-$, and as such, the degenerate diffusion type term requires careful treatment when constructing a numerical solution.

The vapour-only zone $L < z < D$ is more simple. Conservation of mass reads

$$(\rho_{\text{v}} u_{\text{v}})_z = 0, \tag{2.1.17}$$

while conservation of energy reads

$$0 = T_{zz}, \tag{2.1.18}$$

since there is no phase change in the vapour-only region.

Now we examine the boundary and interface conditions required to close the model problem. At $z = D$, we take

$$T = T_1, \tag{2.1.19}$$
$$u_v = 0. \tag{2.1.20}$$

Now, at the free interface, we have the following five conditions:

$$s = 0, \tag{2.1.21}$$
$$[T]_-^+ = 0, \tag{2.1.22}$$
$$[p]_-^+ = 0, \tag{2.1.23}$$
$$(\rho_l u_l + \rho_v u_v)^- = (\rho_v u_v)^+, \tag{2.1.24}$$
$$(\widehat{K} T_z - h_{vap}\rho_v u_v)^- = (\widehat{K} T_z)^+. \tag{2.1.25}$$

At the boundary $z = 0$, we have

$$T = T_0, \tag{2.1.26}$$
$$\rho_l u_l + \rho_v u_v = 0. \tag{2.1.27}$$

In order to find a unique solution, we add the integral constraint

$$\int_0^L (s\rho_l + (1-s)\rho_v)\mathrm{d}z + \int_L^D \rho_v \,\mathrm{d}z = W, \tag{2.1.28}$$

where W is the fixed total water mass per cross sectional area of the porous pack.

2.2. Numerical method and results

The numerical solution method described in [6] is based on one-dimensional integration, reducing the boundary value problems to coupled ordinary differential equations for saturation and temperature in the two-phase region, and temperature and pressure in the vapour region. These ODE's are solved numerically using standard Runge–Kutta time-stepping, and a quasi-Newton method iterates on the heat flux through the porous layer in order to satisfy the global constraint (2.1.28). Here, we extend this method to generate steady-state solutions, allowing for variations in vapour density, according to the ideal gas law. In Fig. 2, we show profiles of saturation and temperature throughout a porous pack of length $D = 0.254$ m, for typical values of temperature and heat flux, and for the data given in Table 1. The interface $L = 0.15$ is clear, as are the derivative discontinuities and the singular saturation gradient.

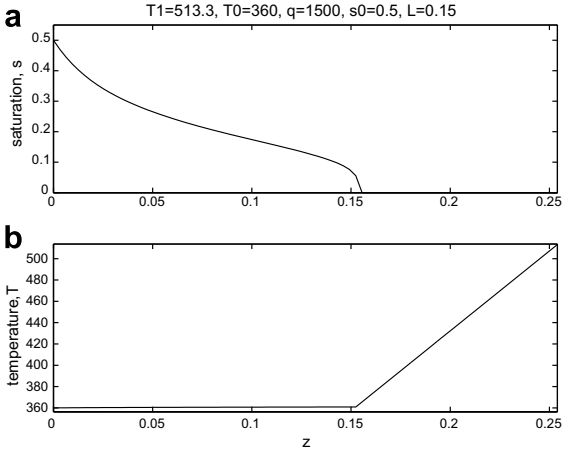

Fig. 2. Steady-state, one-dimensional profiles.

3. The M2 mixture method for the transient Udell problem

In this section, we describe the time-dependent extension of the steady, one-dimensional phase-change problem presented in the previous section. We carefully derive the conditions on the moving interface, and show that these will be difficult to implement in disjoint-domain numerical solution methods which involve front tracking. Clearly, front-capturing methods appeal for this type of problem. We shall describe a reformulation of the problem over a fixed domain, in which the interface conditions are not explicitly imposed. This formulation is similar to the mixture formulation presented by Wang and Beckermann [23], who implement a numerical solution method for the case of an isothermal two-phase region. We describe the finite volume solution of the nonisothermal mixture problem.

3.1. Mathematical formulation of the model problem

Here, we present a model based on the time-dependent extensions to the steady-state conservation equations (2.1.2)–(2.1.4) and (2.1.17) and (2.1.18). Firstly, we consider the two-phase zone $0 < z < L(t)$, where the interface location is now a function of time. In this region, we have conservation of liquid mass. The mass (per unit volume) of liquid in a control volume is $\phi\rho_l s$, where ϕ is the porosity of the medium, ρ_l is the liquid density, and s is the saturation, as before. Then, conservation of liquid mass is given by

$$(\phi\rho_l s)_t + (\rho_l u_l)_z = \Gamma, \tag{3.1.1}$$

where as before, u represents the Darcy velocity, and Γ is the condensation rate. Similarly, conservation of mass for the vapour phase is given by

$$(\phi\rho_v(1-s))_t + (\rho_v u_v)_z = -\Gamma. \tag{3.1.2}$$

The energy equation is now

$$(\overline{\rho c})T_t = \widehat{K}T_{zz} + h_{vap}\Gamma, \tag{3.1.3}$$

with a mass averaged product of density and heat capacity appearing. We assume here that the dominant density–heat capacity product is that of the porous medium, such that we can neglect variations in this quantity with saturation. Certainly, this will be true for small values of saturation near the interface.

As in the steady-state problem, we can eliminate the condensation rate between the three conservation equations to give conservation of mass as

$$\phi(\rho_l s + \rho_v(1-s))_t + (\rho_l u_l + \rho_v u_v)_z = 0, \tag{3.1.4}$$

and

$$(\overline{\rho c})T_t = \widehat{K}T_{zz} - h_{vap}\big((\phi\rho_v(1-s))_t + (\rho_v u_v)_z\big). \tag{3.1.5}$$

Again, we have a coupled system for the two unknowns s and T in the two-phase zone $0 < z < L(t)$.

In the vapour-only region $L(t) < z < D$, there is no condensation, and conservation of mass gives

$$(\phi\rho_v)_t + (\rho_v u_v)_z = 0, \tag{3.1.6}$$

and conservation of energy is given by the heat equation with no source term:

$$(\overline{\rho c})T_t = \widehat{K}T_{zz}. \tag{3.1.7}$$

We now have parabolic systems in two unknowns on either side of the moving interface $z = L(t)$, and, as such, we require five conditions to be specified on the interface. The first three conditions are that saturation is zero, the temperature is continuous, and the vapour pressure is continuous, giving the conditions

$$s = 0, \tag{3.1.8}$$

$$[T]^+_- = 0, \tag{3.1.9}$$

$$[p]^+_- = 0, \tag{3.1.10}$$

which are exactly the same as conditions (2.1.21)–(2.1.23). The two remaining conditions again come from conservation of mass and energy across the interface. These conditions require careful consideration of the effect of the nonzero velocity of the interface, and we derive these conditions in the following subsection.

3.2. Modified Stefan conditions at the interface $z = L(t)$

The well-known Stefan condition describes conservation of energy across a freezing/melting interface moving through a body of water, say, separating regions of liquid and solid. Crank [7] presents a derivation of this condition. The major assumptions which are made are that the water density is the same in either phase, and that the water in each phase is stationary. Clearly, the Stefan condition must be modified for problems in which there is an interface between liquid and vapour phases, where the fluid on either side of the interface may be moving, and in cases where additional heat sources or sinks exist. With this in mind, we now find conditions for mass and energy conservation across the interface, in terms of the interface velocity $\dot{L}(t)$.

Firstly, we consider conservation of mass across a general moving interface which separates two fluids, possibly different phases, which may have different densities and velocities. The argument is presented for a one-dimensional problem, which is shown in Fig. 3. The fluid to the left of the interface has density ρ_{I}, and is moving with velocity u_{I}, while the fluid to the right of the interface has density ρ_{II}, and is moving with velocity u_{II}. Suppose that the interface moves a distance δz in short time δt, and that it moves with velocity $\dot{L}(t)$. Mass conservation requires that the difference between the mass in the control volume $[L(t), L(t) + \delta z]$ over the time interval $[t, t + \delta t]$ is due to the net mass flux into the control volume during that interval. For the problem shown in Fig. 3, this gives

$$(\rho_{\mathrm{I}} - \rho_{\mathrm{II}})\delta z = (\rho_{\mathrm{l}} u_{\mathrm{I}} - \rho_{\mathrm{II}} u_{\mathrm{II}})\delta t.$$

Taking the limit as $\delta t \to 0$, we arrive at a condition on the velocity of the interface, that is

$$(\rho_{\mathrm{I}} - \rho_{\mathrm{II}})\dot{L}(t) = \rho_{\mathrm{I}} u_{\mathrm{I}} - \rho_{\mathrm{II}} u_{\mathrm{II}}. \tag{3.2.1}$$

Further, in the case of flow through a porous medium which has porosity ϕ, the interface velocity will be given by

$$\phi(\rho_{\mathrm{I}} - \rho_{\mathrm{II}})\dot{L}(t) = \rho_{\mathrm{I}} u_{\mathrm{I}} - \rho_{\mathrm{II}} u_{\mathrm{II}}, \tag{3.2.2}$$

where u_{I} and u_{II} are now understood to be the Darcy velocities. Now, for the Udell phase-change problem, suppose we take region I to be the two-phase region, and region II to be the vapour-only region. The condition (3.2.2) holds, but we must consider *mixture* quantities in region I. That is, we consider quantities associated with the mixture of liquid and vapour in the two-phase region. Let us define

$$\begin{aligned} &\rho_{\mathrm{I}} = \rho_{\mathrm{l}} s + \rho_{\mathrm{v}}(1 - s), \quad \text{the mixture density,} \\ &\rho_{\mathrm{I}} u_{\mathrm{I}} = \rho_{\mathrm{l}} u_{\mathrm{l}} + \rho_{\mathrm{v}} u_{\mathrm{v}}, \quad \text{the mixture mass flux.} \end{aligned} \tag{3.2.3}$$

Then Eq. (3.2.2) gives

$$\phi\big((\rho_{\mathrm{l}} s + \rho_{\mathrm{v}}(1 - s))_{\mathrm{I}} - (\rho_{\mathrm{v}})_{\mathrm{II}}\big)\dot{L}(t) = (\rho_{\mathrm{l}} u_{\mathrm{l}} + \rho_{\mathrm{v}} u_{\mathrm{v}})_{\ \mathrm{I}} - (\rho_{\mathrm{v}} u_{\mathrm{v}})_{\mathrm{II}}.$$

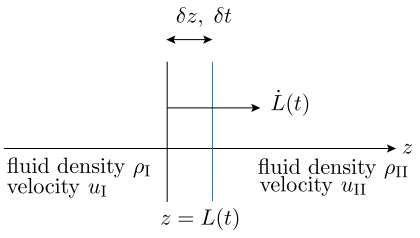

Fig. 3. Mass conservation at the moving interface.

Now, in view of the continuity of temperature (3.1.9) and of vapour pressure (3.1.10), we have that $(\rho_v)_I - (\rho_v)_{II} = 0$, and hence

$$\phi((\rho_l - \rho_v)s)_I \dot{L}(t) = (\rho_l u_l + \rho_v u_v)_I - (\rho_v u_v)_{II}. \tag{3.2.4}$$

To explicitly find the interface velocity, we must be careful. Specifically, the saturation condition at the interface (3.1.8) is $s = 0$ at $z = L^-$. The velocity $\dot{L}(t)$ must be considered as a limit of an indeterminate form. In particular, the velocity is explicitly given by

$$\dot{L}(t) = \lim_{z \to L(t)^-} \frac{(\rho_l u_l + \rho_v u_v)_I - (\rho_v u_v)_{II}}{\phi(\rho_l - \rho_v)_I s}. \tag{3.2.5}$$

We note that such an indeterminate form for the velocity of a moving interface, resulting from a mass conservation argument, also arises when considering the porous medium equation. A common feature here is the degeneracy as $s \to 0$.

Now, for the Udell phase-change problem, we also require an energy balance across the moving interface, which we will also see to be a limit of an indeterminate form. The argument we present here is an extension of Crank's [7] derivation of the Stefan condition in one dimension. Our problem includes an extra term due to motion and phase change in the two-phase region, and we refer to the energy balance as a *Modified Stefan Condition*. Consider the problem shown in Fig. 4. The interface between the two-phase region and the vapour-only region in the Udell problem moves a small distance δz in the small time interval δt. The heat which flows into the control volume during the time interval is

$$\left(\widehat{K}\frac{\partial T}{\partial z}\right)_{II} \delta t,$$

while the heat which flows out of the control volume during the time interval is

$$\left(\widehat{K}\frac{\partial T}{\partial z}\right)_{I} \delta t.$$

Now, the heat required to evaporate the liquid which moves up to the interface is

$$(h_{vap}\rho_l u_l)\delta t.$$

These three quantities are exactly the same as for the steady-state problem. We now consider the extra heat released or required when the interface moves.

First consider the case $\delta z, \dot{L} > 0$. The additional mass which appears in the two-phase zone after the interface has moved is $\phi s \rho_l \delta z$. This must be exactly the amount of mass from region II which has condensed, and the heat released upon condensation is then

$$h_{vap}\phi s \rho_l \delta z.$$

Given these four terms, we see that the energy balance across the interface is given by

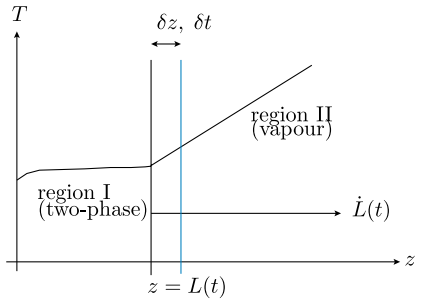

Fig. 4. Temperature profile and the moving interface.

$$\left[\widehat{K}\frac{\partial T}{\partial z}\right]_{\mathrm{I}}^{\mathrm{II}}\delta t + h_{\mathrm{vap}}\phi s\rho_{\mathrm{l}}\delta z = h_{\mathrm{vap}}\rho_{\mathrm{l}}u_{\mathrm{l}}\delta t.$$

Now, we take the limit as $\delta z, \delta t \to 0$ to give

$$h_{\mathrm{vap}}\phi s\rho_{\mathrm{l}}\dot{L}(t) = h_{\mathrm{vap}}\rho_{\mathrm{l}}u_{\mathrm{l}} - \left[\widehat{K}\frac{\partial T}{\partial z}\right]_{\mathrm{I}}^{\mathrm{II}}. \tag{3.2.6}$$

To find $\dot{L}(t)$, we note that $s \to 0^+$ as $z \to L(t)^-$, and evaluate the limit

$$\dot{L}(t) = \lim_{z\to L(t)^-}\left\{\frac{h_{\mathrm{vap}}\rho_{\mathrm{l}}u_{\mathrm{l}} - \left[\widehat{K}\frac{\partial T}{\partial z}\right]_{\mathrm{I}}^{\mathrm{II}}}{h_{\mathrm{vap}}\phi s\rho_{\mathrm{l}}}\right\}. \tag{3.2.7}$$

Now, if we repeat this argument for the case $\delta z, \dot{L} < 0$, we get exactly the same condition. Notice that, if we take (3.2.7) as the indeterminate modified Stefan condition which determines the interface velocity, then the mass balance (3.2.5) becomes

$$(\rho_{\mathrm{l}}u_{\mathrm{l}} + \rho_{\mathrm{v}}u_{\mathrm{v}})_{\mathrm{I}} - (\rho_{\mathrm{v}}u_{\mathrm{v}})_{\mathrm{II}} = \frac{(\rho_{\mathrm{l}} - \rho_{\mathrm{v}})_{\mathrm{I}}\left\{h_{\mathrm{vap}}(\rho_{\mathrm{l}}u_{\mathrm{l}})_{\mathrm{I}} - \left[\widehat{K}\frac{\partial T}{\partial z}\right]_{\mathrm{I}}^{\mathrm{II}}\right\}}{h_{\mathrm{vap}}\rho_{\mathrm{l}}}, \quad \text{as } z \to L^-. \tag{3.2.8}$$

We note here that the indeterminate modified Stefan conditions (3.2.5) and (3.2.7) can be thought of as limiting cases of the Rankine–Hugoniot conditions for our system (see, for example [1]), but we include the careful derivation here.

3.3. Model summary

In summary, we have a two-phase region $0 < z < L(t)$, in which

$$\phi(\rho_{\mathrm{l}}s + \rho_{\mathrm{v}}(1-s))_t + (\rho_{\mathrm{l}}u_{\mathrm{l}} + \rho_{\mathrm{v}}u_{\mathrm{v}})_z = 0, \tag{3.3.1}$$

and

$$(\overline{\rho c})T_t = \widehat{K}T_{zz} - h_{\mathrm{vap}}\big((\phi\rho_{\mathrm{v}}(1-s))_t + (\rho_{\mathrm{v}}u_{\mathrm{v}})_z\big). \tag{3.3.2}$$

The vapour-only region $L(t) < z < D$ has

$$(\phi\rho_{\mathrm{v}})_t + (\rho_{\mathrm{v}}u_{\mathrm{v}})_z = 0, \tag{3.3.3}$$

and

$$(\overline{\rho c})T_t = \widehat{K}T_{zz}. \tag{3.3.4}$$

At the moving interface $z = L(t)$, the five conditions are

$$s = 0, \tag{3.3.5}$$

$$[T]_-^+ = 0, \tag{3.3.6}$$

$$[p]_-^+ = 0, \tag{3.3.7}$$

$$\phi((\rho_{\mathrm{l}} - \rho_{\mathrm{v}})s)_{\mathrm{I}}\dot{L}(t) = (\rho_{\mathrm{l}}u_{\mathrm{l}} + \rho_{\mathrm{v}}u_{\mathrm{v}})_{\mathrm{I}} - (\rho_{\mathrm{v}}u_{\mathrm{v}})_{\mathrm{II}}, \tag{3.3.8}$$

$$h_{\mathrm{vap}}\phi s\rho_{\mathrm{l}}\dot{L}(t) = h_{\mathrm{vap}}\rho_{\mathrm{l}}u_{\mathrm{l}} - \left[\widehat{K}\frac{\partial T}{\partial z}\right]_{\mathrm{I}}^{\mathrm{II}}. \tag{3.3.9}$$

At the upper boundary $z = D$, we impose a temperature $T = T_1$, and have no mass flux, so that $u_v = 0$. At the lower boundary $z = 0$, we impose a temperature $T = T_0 (< T_1)$, and have no mass flux, so that $\rho_{\mathrm{l}}u_{\mathrm{l}} + \rho_{\mathrm{v}}u_{\mathrm{v}} = 0$. Finally, we give initial profiles of saturation, temperature and pressure throughout the entire system at time $t = 0$.

3.4. Fixed domain, mixture formulation

Any numerical method which is based on solutions in the disjoint domains $0 < z < L(t)$ and $L(t) < z < D$ will require an implementation of the interface conditions. A natural approach to take is that of front tracking, which requires that the interface velocity be imposed explicitly. Suppose we were to take the interface condition (3.3.8) as the condition which defines the velocity $\dot{L}(t)$. Any explicit implementation of this will require evaluation of the indeterminate form given in (3.2.5). Thus, any front-tracking scheme requires not only the explicit computation of interface location at each time step, but an accurate numerical evaluation of this limit. Furthermore, extension of a front-tracking scheme to higher dimensions would also require consideration of the interface geometry, and solutions to problems on irregular domains.

Clearly, front tracking is not feasible for this model problem. An alternative is to reformulate the problem over the fixed domain $0 < z < D$, thereby avoiding the need for explicit consideration of the complex interface physics. The interface location can be recovered, *a posteriori*, from the solution of the transient, fixed-domain problem. Such an approach is referred to as a *front-capturing* method. Here, we present a reformulation based on the mixture model described by Wang and Beckermann [23].

The reformulation is in terms of a density over the entire pack, rather than saturation in just the two-phase zone. The main point is that if we consider the water anywhere in the porous pack to be a mixture of vapour and liquid, then the density of this mixture must be continuous, even as we cross the interface. Suppose we define the *mixture density* ρ by

$$\rho = \rho_l s + \rho_v (1 - s). \tag{3.4.1}$$

Then Eqs. (3.3.1) and (3.3.2) reduce to the system

$$\left.\begin{aligned} \phi \rho_t &= -(\rho_l u_l + \rho_v u_v)_z \\ (\overline{\rho c}) T_t &= \widehat{K} T_{zz} - h_{vap}\big((\phi \rho_v (1-s))_t + (\rho_v u_v)_z\big) \end{aligned}\right\}. \tag{3.4.2}$$

Now, the variables u_v, u_l, ρ_v are all functions of s and T, and in particular

$$u_v = \frac{-\kappa}{\mu_v}(1-s)^3\left(\frac{\partial p_v}{\partial z} + \rho_v g\right), \tag{3.4.3}$$

$$u_l = \frac{-\kappa}{\mu_l} s^3 \left(\frac{\partial}{\partial z}(p_v - \delta J(s)) + \rho_l g\right), \tag{3.4.4}$$

and

$$J(s) = 1.417(1-s) - 2.120(1-s)^2 + 1.263(1-s)^3, \tag{3.4.5}$$

where p_v is the vapour pressure. So if ρ_v, p_v, s can be found as functions of ρ and T, then (3.4.2) is a system in the two dependent variables ρ and T. Furthermore, given that ρ is the density of the liquid–vapour mixture, the system (3.4.2) is valid over the entire porous pack, rather than just the two-phase zone. Thus, we seek solutions to (3.4.2), from which we can recover the position of the interface between the two-phase zone and the vapour-only zone.

Now that we are considering a system valid over the entire domain, we can not take the vapour pressure to be equal to the saturation pressure. Rather, the vapour pressure at a point will be equal to either the saturation pressure (in which case, the point is in the two-phase zone) or the pressure given by the ideal gas law for the vapour-only zone. Given values of ρ and T, a comparison of these two pressures, namely

$$p_{sat}(T) = a e^{bT}, \qquad p^*(\rho, T) = \frac{\rho R T}{M},$$

determines whether or not the vapour is fully saturated, and hence the values of p_v, ρ_v and s. If $p^* < p_{sat}$, then the vapour is undersaturated, so must be in the vapour-only region. In this case, the vapour pressure $p = p^*$. If $p_{sat} < p^*$, then the vapour is fully saturated, and hence $p = p_{sat}$. We see that Eqs. (3.4.2), together with the algebraic constraint

$$p_{\mathrm{v}} = \min\left(p_{\mathrm{sat}}(T), \frac{\rho RT}{M}\right), \tag{3.4.6}$$

form a differential-algebraic system for the two variables ρ, T, which is valid over the entire domain. The map (3.4.6) is the crux of our reformulation, and we name this the *M2-map*.

3.5. Numerical method and results

Eqs. (3.4.1)–(3.4.6) give a coupled parabolic system on the domain $0 < z < D$. Now we consider the discretization of the problem, written as

$$\rho_t - \frac{\partial}{\partial z} q\left(\rho, T, \frac{\partial}{\partial z}\right) = 0, \tag{3.5.1}$$

$$\overline{\rho c} T_t + w(\rho, T)_t = \frac{\partial}{\partial z} Q\left(\rho, T, \frac{\partial}{\partial z}\right), \tag{3.5.2}$$

where the fluxes q, Q are given by

$$q\left(\rho, T, \frac{\partial}{\partial z}\right) = \frac{\kappa}{\phi}\left(f_{\mathrm{A}}(\rho, T)\frac{\partial}{\partial z} g_{\mathrm{A}}(\rho, T) + f_{\mathrm{B}}(\rho, T)\frac{\partial}{\partial z} g_{\mathrm{B}}(\rho, T)\right), \tag{3.5.3}$$

$$Q\left(\rho, T, \frac{\partial}{\partial z}\right) = \widehat{K} T_z + \frac{h_{\mathrm{vap}}\kappa}{\mu_v} f_C(\rho, T)\frac{\partial}{\partial z} g_C(\rho, T), \tag{3.5.4}$$

where

$$\begin{aligned}
f_{\mathrm{A}}(\rho, T) &= \frac{\rho_l}{\mu_l} s^3 + \frac{\rho_{\mathrm{v}}}{\mu_{\mathrm{v}}}(1-s)^3,\\
g_{\mathrm{A}}(\rho, T) &= p,\\
f_{\mathrm{B}}(\rho, T) &= \frac{\rho_{\mathrm{l}}}{\mu_{\mathrm{l}}}\delta,\\
g_{\mathrm{B}}(\rho, T) &= \psi(s),\\
f_{\mathrm{C}}(\rho, T) &= \rho_{\mathrm{v}}(1-s)^3,\\
g_{\mathrm{C}}(\rho, T) &= p,
\end{aligned}$$

and the function w is given by

$$w(\rho, T) = h_{\mathrm{vap}}\phi\rho_{\mathrm{v}}(1-s). \tag{3.5.5}$$

The time-dependent terms in the energy equation have been grouped together, leaving the time derivative of an enthalpy-type quantity. Also, in keeping with formulations of degenerate diffusion problems for numerical computation [10], we have rewritten the degenerate liquid velocity as

$$\mathbf{u}_{\mathrm{l}} = -\frac{\kappa}{\mu_{\mathrm{l}}}\left(s^3 p_z + \delta(\psi(s))_z\right), \tag{3.5.6}$$

where the function ψ is given by

$$\psi(s) = -\int^s \xi^3 J'(\xi)\mathrm{d}\xi = 0.2415 s^4 - 0.6676 s^5 + 0.6315 s^6. \tag{3.5.7}$$

This change-of-variables idea is used in preference to regularisations of the type $\kappa_{rl} = s^3 + \eta$, such as those seen in the fuel cell literature [14,15]. The numerical convenience offered by such regularisations is due to the fact that they smear out the sharp interface. The interface in the continuous problem is smeared in space over a width $\mathcal{O}(\eta)$, introducing errors before the discretization. The effect of such smearing is demonstrated for a simple scalar problem in Appendix A.

Also, we have the boundary conditions

$$q|_{z=0} = q_{\text{bot}}(t), q|_{z=D} = q_{\text{top}}(t), T|_{z=0} = T_{\text{bot}}(t), T|_{z=D} = T_{\text{top}}(t). \tag{3.5.8}$$

For the closed sand pack, the boundary fluxes are zero, and we will take the boundary temperatures to be constant in time. Now we wish to implement a numerical scheme for the solution of the system (3.5.1)–(3.5.8). Two implementation options are available for explicit time-stepping. One option is to use a quasi-enthalpy method. The density ρ may be explicitly updated from the mass Eq. (3.5.1). Then the *enthalpy* E, defined by

$$E(\rho, T) = \overline{\rho c} T + w(\rho, T), \tag{3.5.9}$$

may be explicitly updated from the energy Eq. (3.5.2). The temperature T must then be recovered from the enthalpy by way of a nonlinear solver. A second option is to form a mass matrix, and write the system (3.4.2) as

$$\begin{pmatrix} a_{11} & a_{12} \\ a_{21} & a_{22} \end{pmatrix} \begin{pmatrix} \rho \\ T \end{pmatrix}_t = \begin{pmatrix} -(\rho_l u_l + \rho_v u_v)_z \\ \widehat{K} T_{zz} - h_{\text{vap}} (\rho_v u_v)_z \end{pmatrix}, \tag{3.5.10}$$

where

$$a_{11} = \phi, \qquad a_{12} = 0,$$

together with

$$a_{21} = h_{\text{vap}} \phi \left((1 - s) \frac{\partial \rho_v}{\partial \rho} - \rho_v \frac{\partial s}{\partial \rho} \right),$$

and

$$a_{22} = \overline{\rho c} + h_{\text{vap}} \phi \left((1 - s) \frac{\partial \rho_v}{\partial T} - \rho_v \frac{\partial s}{\partial T} \right).$$

Either of these two explicit methods requires the computation of derivatives of all quantities with respect to the primary variables ρ, T, as would an implicit method. Given the inherent stiffness in the problem, here we shall use a fully implicit scheme. Now we discretize the parabolic problem (3.5.1)–(3.5.8) by finite volumes, in order to conserve the total mass, given by

$$\int_0^D \rho(z, t) \mathrm{d}z,$$

in a discrete sense.

Given that mass flux is given at the boundaries (3.5.8), we develop a scheme which computes a discrete approximation to the solution of (3.5.1) and (3.5.2) with mass fluxes on a grid which coincides with the boundary points, and density ρ on the corresponding staggered grid. That is, we use a finite volume scheme for updating ρ_j, which is the cell average density for cell j. Also, we use cell averaged temperatures. Consider Fig. 5. Let τ_j and ρ_j be the average values of temperature, T, and density, ρ respectively, over grid cell j. We introduce vectors $\mathbf{T}$ and $\mathbf{R}$ to represent the interpolated values of temperature T and density ρ falling on the grid. So we have

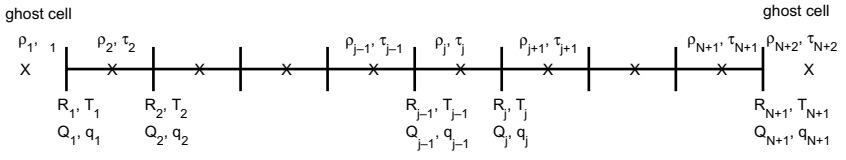

Fig. 5. Grid and staggered grid.

$$\begin{aligned} T_j &= \tau_{j+1/2} = \frac{\tau_j + \tau_{j+1}}{2} \quad \text{for } j = 1, \ldots, N+1, \\ R_j &= \rho_{j+1/2} = \frac{\rho_j + \rho_{j+1}}{2} \quad \text{for } j = 1, \ldots, N+1. \end{aligned} \tag{3.5.11}$$

Then a fully implicit (Backward Euler), conservative, finite volume scheme for the mass Eq. (3.5.1) is given by the discretization

$$F_j = \frac{\rho_j^{n+1} - \rho_j^n}{k} - \frac{1}{h}\left(q_j - q_{j-1}\right)^{n+1} = 0, \quad j = 2, \ldots, N+1, \tag{3.5.12}$$

where the discrete fluxes are given by

$$\begin{aligned} q_j = \frac{\kappa}{\phi}\left(f_{\mathrm{A}}(R_j, T_j)\left(\frac{g_{\mathrm{A}}(\rho_{j+1}, \tau_{j+1}) - g_{\mathrm{A}}(\rho_j, \tau_j)}{h}\right) + f_{\mathrm{B}}(R_j, T_j)\left(\frac{g_{\mathrm{B}}(\rho_{j+1}, \tau_{j+1}) - g_{\mathrm{B}}(\rho_j, \tau_j)}{h}\right)\right), \\ j = 1, \ldots, N+1, \end{aligned} \tag{3.5.13}$$

Next, we discretize the energy Eq. (3.5.2) in a similar manner. We have

$$G_j = \overline{\rho c}\,\frac{\tau_j^{n+1} - \tau_j^n}{k} + \frac{w(\rho_j^{n+1}, \tau_j^{n+1}) - w(\rho_j^n, \tau_j^n)}{k} - \frac{1}{h}\left(Q_j - Q_{j-1}\right)^{n+1} = 0, \quad j = 2, \ldots, N+1, \tag{3.5.14}$$

where

$$Q_j = \widehat{K}\,\frac{\tau_{j+1} - \tau_j}{h} + \frac{h_{\mathrm{vap}}\kappa}{\mu_{\mathrm{v}}} f_{\mathrm{C}}(R_j, T_j)\left(\frac{g_{\mathrm{C}}(\rho_{j+1}, \tau_{j+1}) - g_{\mathrm{C}}(\rho_j, \tau_j)}{h}\right), \quad j = 1, \ldots, N+1. \tag{3.5.15}$$

Here, k, h are the chosen time step and grid spacing, and superscripts denote the time level. The boundary conditions give

$$\begin{aligned} F_1 &= q_1 - q_{\mathrm{bot}} = 0, \\ G_1 &= T_1 - T_{\mathrm{bot}} = 0, \\ F_{N+2} &= q_{N+1} - q_{\mathrm{top}} = 0, \\ G_{N+2} &= T_{N+1} - T_{\mathrm{top}} = 0. \end{aligned} \tag{3.5.16}$$

Note that we cannot find the ghost values ρ_1, ρ_{N+2} explicitly in terms of interior cell values, so we just include them in the system to be solved. That is, we have $2(N+2)$ nonlinear equations

$$F_j = 0, \quad G_j = 0, \quad j = 1, \ldots, N+2,$$

for the unknowns $\rho_j, \tau_j, j = 1, \ldots, N+2$. We use a Newton method with analytical Jacobian. An alternative method described by Knoll et al. [12] for scalar Stefan problems achieves Newton-like convergence without explicitly forming the Jacobian. It is unclear as yet whether such an approach could be applied here. We replace the nonsmooth map (3.4.6) with the smoothed minimum

$$p = \widetilde{\min}_{\varepsilon}(p_{\mathrm{sat}}, p^*) = \widetilde{H}_{\varepsilon}(p^* - p_{\mathrm{sat}})p_{\mathrm{sat}} + (1 - \widetilde{H}_{\varepsilon}(p^* - p_{\mathrm{sat}}))p^*, \tag{3.5.17}$$

where the smoothed Heaviside function is given by

$$\widetilde{H}_{\varepsilon}(X) = \frac{1}{2}\left\{1 + \tanh\left(\frac{X}{\varepsilon}\right)\right\}, \tag{3.5.18}$$

for a smoothing radius ε, and $p^* = \frac{R}{M}\rho T$. In practice, the smoothing radius ε can be taken arbitrarily small, ie. to machine precision. This replacement is thus merely a coding convenience used in order to avoid "if" statements; the singularity and degeneracy in the saturation equation are retained.

In Fig. 6, we show a typical result, starting from an initial uniform density, with no mass flux across the boundaries. The initial temperature is uniform, and the system is subject to sudden heating up to a fixed temperature at the upper boundary. A number of density, temperature and saturation profiles are shown, for increasing time, and we note that the profiles shown approach the correct steady-state profiles. The transition

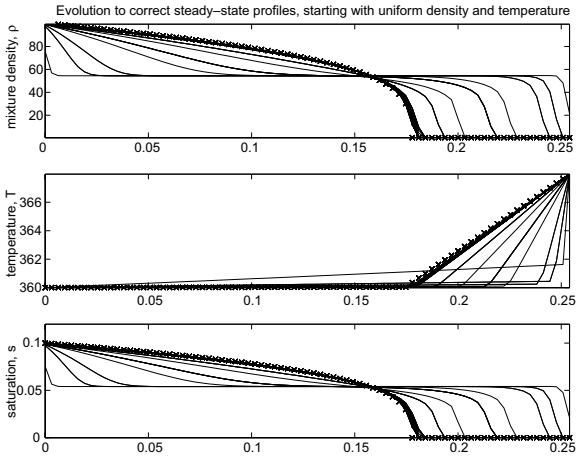

Fig. 6. Evolution to correct steady state.

to an interface $s = 0$ is captured, and the interface between the two-phase and vapour regions is clearly moving to the left. In Fig. 7, the interface position, $L(t)$ is plotted. The stepwise behaviour is due to the discretization, and the fact that we take $L(t)$ as the first grid point to the right of $s = 0$. Also, we plot $L(t)$ for three grid sizes: $N = 20, 40, 80$. Convergence to a base numerical solution is clear as the grid is refined. The question remains, however, of whether the numerical method indeed computes the interface velocity accurately. This will be addressed in the following section.

Fig. 8 shows the temperature history at a point. An initial increase in temperature is numerically the result of the sudden-heating boundary condition. After this, the temperature history has a wavy, stepwise nature, in common with the enthalpy-method solution of the Stefan problem [1]. For the Stefan problem, a control volume is held at the fixed phase-change temperature while the interface moves through it. Another way of saying that is that the temperature remains fixed while the enthalpy in that control volume increases/decreases through the latent heat jump. The staircasing then is a result of successive temperature relaxations. For our problem, there is no jump in enthalpy. We believe that the staircasing here is due to liquid water movement occurring on a much longer timescale than temperature change, so that when the interface initially enters a control volume, the temperature rapidly changes, then slowly relaxes as the cell accumulates water and the discrete saturation profile steepens. Quantitative analysis of this staircasing phenomenon is suggested as future work.

For the results shown in Figs. 6–8, small time steps are initially required, in order for the Newton iteration to converge to within the specified tolerance. In fact, initially, we use Forward Euler time-stepping to get past the initial transients, and then employ the fully implicit scheme. However, the time step required for convergence to within a fixed tolerance decreases as the saturation profile steepens before the interface moves by a grid point. In Fig. 9, we demonstrate the stiffness in the problem. An experiment was performed using implicit

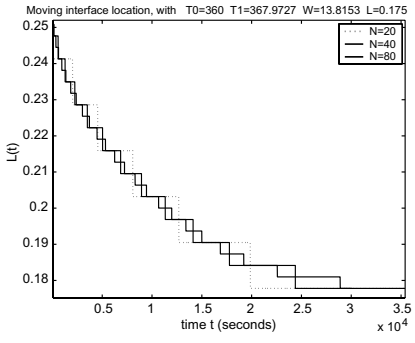

Fig. 7. Interface location $L(t)$, with grid refinement.

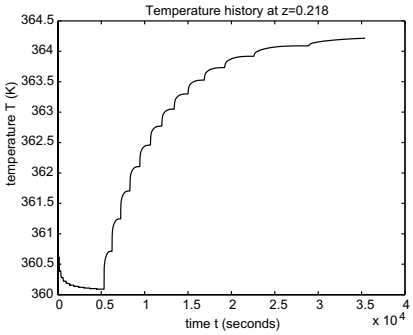

Fig. 8. Temperature history at a point.

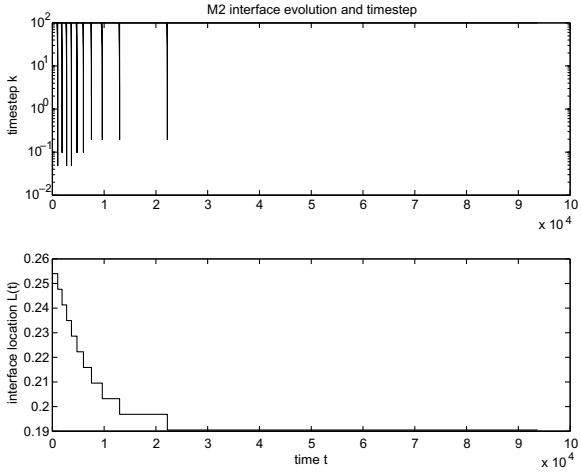

Fig. 9. Timestep and interface location.

time-stepping with adaptive time-step. Whenever the nonlinear solver is unable to converge to within the required tolerance, the time-step is halved. The figure clearly shows the relationship between the time-step and the interface advance.

4. Numerical convergence studies

Numerical experiments using our mixture-based capturing method for the time-dependent problem show that initial distributions evolve to the correct steady-state solutions, as given by the method of Section 3. We now examine the dynamics of the system to ensure that the method indeed captures the moving interface accurately in space and time. Typically, the convergence of numerical methods for moving boundary problems is demonstrated using initial and boundary data consistent with known similarity solutions. Similarity solutions are available for the two-phase Stefan problem and the porous medium equation. In the literature, similarity solutions have been found for reduced, scalar models of phase change in porous media (see, for example, [26]). Here, we reduce our model problem only by simplifying the coefficients, but we retain the full, nonlinear, vector problem, and construct a travelling wave solution.

4.1. The full Udell problem

Consider computations where the number of grid cells is N, and num is the number of time steps. We quantify the errors by calculating numerically the norms of the errors made in the temperature T, the mixture density ρ, and the interface location L. Specifically, we compute the time-averaged quantities defined by

$$\|E_T\|_1 = \frac{1}{\text{num}}\frac{1}{N}\sum_{n=1}^{\text{num}}\sum_{j=1}^{N}\left|T(z_j,t_n) - T_{\text{exact}}(z_j,t_n)\right|,$$

$$\|E_\rho\|_1 = \frac{1}{\text{num}}\frac{1}{N}\sum_{n=1}^{\text{num}}\sum_{j=1}^{N}\left|\rho(z_j,t_n) - \rho_{\text{exact}}(z_j,t_n)\right|,$$

with reference to exact solutions.

For the full system (3.3.1)–(3.3.9), exact analytical solutions are unavailable, and instead we take use a base numerical solution using $N = 320$ and num = 25,600 as an exact solution. The initial condition for our study is a two-phase/vapour system with an interface $L \approx 0.2$. In Table 2, we show the results of a numerical convergence study, keeping $\mu = k/h^2$ fixed. As the grid spacing is halved, the temperature and density errors decrease by factors of around 2.2 and 2.5, respectively. While second-order accuracy in space is not achieved, this is not to be expected since lower order errors are introduced near the interface. However, convergence is clear at around first-order, and compares well with enthalpy-method solution of the scalar Stefan problem, and Evje's method for the Porous Medium Equation, which are both also around first-order accurate. We note here that fixing the grid spacing and varying the time step hardly effects the computed errors – the spatial error is dominant. We will shortly present a temporal convergence study.

4.2. A reduced model problem

While the base numerical solutions for the full problem allow a convergence study, we now seek analytical solutions to a reduced problem. These new solutions are constructed for use in further convergence studies presented here, but also with a view to more analytical questions to be answered in future work.

Let us consider a model problem with reduced Darcy velocities, and the majority of coefficients equal to one. Specifically, we consider

$$\text{liquid flux} = -\rho_l s^3(p_z + s_z), \quad \text{and} \quad \text{vapour flux} = -\rho_v p_z,$$

where we have simplified the Leverett function and the relative permeability, and have taken absolute permeability and viscosity to be unity. We note that removing the relative permeability of vapour, namely $(1-s)^3$, will not affect the singularity structure at $s = 0$, but it will allow for solutions with saturation $s > 1$. In this sense, the solutions cease to be physically meaningful. Conservation of liquid mass reads

$$(\rho_l s)_t - \left(\rho_l s^3(s_z + p_z)\right)_z = \Gamma. \tag{4.2.1}$$

Conservation of vapour mass reads

$$(\rho_v)_t - (\rho_v p_z)_z = -\Gamma, \tag{4.2.2}$$

where the weighting $(1-s)$ has been taken as 1. Again, this will not affect the structure near $s = 0$. Conservation of energy is

$$T_t = T_{zz} + \Gamma. \tag{4.2.3}$$

In the vapour region, we have

$$\Gamma \equiv 0, \quad p = \rho_v T \text{ (ideal gas)}, \quad p < p_{\text{sat}}(T) \text{ (undersaturated)}, \quad s \equiv 0,$$

leaving a problem for ρ_v, T (or p, T). In the two-phase region, we have

Table 2
Errors for full Udell model

N	num	$\|E_T\|_1$	fac	$\|E_\rho\|_1$	fac
20	100	4.1712 E − 2		8.0711 E − 1	
40	400	1.9847 E − 2	2.10	3.0720 E − 1	2.63
80	1600	8.9544 E − 3	2.22	1.2131 E − 1	2.53

Base solution has $N = 320$, with $k = 0.25, \text{num} = 25,600$.

$$p = \rho_v T \text{ (ideal gas)}, \quad p = p_{sat}(T) \text{ (fully saturated)},$$

leaving a problem for s, T and Γ. At the interface $z = L(t)$, we have five conditions, corresponding to (3.3.5)–(3.3.9):

$$s = 0, \tag{4.2.4}$$

$$[T]_-^+ = 0, \tag{4.2.5}$$

$$[p]_-^+ = 0, \tag{4.2.6}$$

$$\text{(Mass) } \rho_l s^- \dot{L}(t) = -\left(\rho_l s^3 (s_z + p_z) + \rho_v p_z\right)^- + \left(\rho(\rho T)_z\right)^+, \tag{4.2.7}$$

$$\text{(Energy) } \rho_l s^- \dot{L}(t) = \left(-\rho_l s^3 (s_z + p_z)\right)^- - [T_z]_-^+. \tag{4.2.8}$$

Note that, in view of the ideal gas law $p = \rho_v T$, conditions (4.2.5) and (4.2.6) further imply continuity of vapour density

$$[\rho_v]_-^+ = 0. \tag{4.2.9}$$

Also, for convenience later, we note that (4.2.7) and (4.2.8) give

$$0 = -(\rho_v p_z)^- + (\rho(\rho T)_z)^+ + [T_z]_-^+. \tag{4.2.10}$$

Then, the five conditions (4.2.4), (4.2.5), (4.2.9), (4.2.8) and (4.2.10) can be used to solve the problem. For the fixed-domain problem on $0 < z < D$, first we define the mixture density

$$\rho = \rho_l s + \rho_v, \tag{4.2.11}$$

and then use the "M2-map"

$$\begin{aligned} p &= \min(\rho T, p_{sat}(T)), \\ \rho_v &= \frac{p}{T}, \\ s &= \frac{\rho - \rho_v}{\rho_l}, \end{aligned} \tag{4.2.12}$$

leaving the coupled system

$$\left.\begin{aligned} &\rho_t - (\rho_l s^3 (s_z + p_z) + \rho_v p_z)_z = 0, \\ &(T + \rho_v)_t = T_{zz} + (\rho_v p_z)_z. \end{aligned}\right\} \tag{4.2.13}$$

In [5], $p_{sat}(T) = \alpha T, \alpha T + \beta, \alpha T + \beta T^2$ are given as three saturation pressure functions of interest which yield semi-analytical travelling wave solutions.

4.2.1. Travelling wave solution for case $p_{sat}(T) = \alpha T$

Suppose the saturation pressure is a linear function of temperature, such that $p_{sat}(T) = \alpha T$. Then $\rho_v \equiv \alpha$ in the two-phase region. Also suppose that we have an infinite porous medium $-\infty < z < \infty$, with far-field temperatures not yet specified. At time t, let there be an interface at $z = ct$ separating a two-phase region $z < ct$, and a vapour-only region $z > ct$. So the interface initially is at $z = 0$, that is, $L(0) = 0$, and we seek travelling wave solutions with speed c. In the two-phase zone, seek solutions

$$s(z,t) = G(\xi), \quad T(z,t) = F_1(\xi), \tag{4.2.14}$$

and, in the vapour zone, seek solutions

$$\rho(z,t) = R(\xi), \quad T(z,t) = F_2(\xi), \tag{4.2.15}$$

where

$$\xi = z - ct. \tag{4.2.16}$$

With $c > 0$ we have wavefronts moving to the right with speed c. As shown in [5], we can construct the following travelling wave solution.

$$F_1(\xi) = A_1 + B_1 \mathrm{e}^{-\frac{c}{1+\alpha^2}\xi}, \tag{4.2.17}$$

$$F_2(\xi) = A_2 + B_2 \mathrm{e}^{-c\xi}, \tag{4.2.18}$$

and $G(\xi) = w^{1/4}(\xi)$, where w solves

$$\frac{1}{4}w' = -\left(cw^{1/4} + \alpha\left(w^{3/4} + \frac{\alpha}{\rho_l}\right)F_1' + A_3\right), \quad \xi \leqslant 0, \;\; w(0) = 0, \tag{4.2.19}$$

and finally, $R(\xi)$ solves

$$R' = -\frac{1}{RF_2(\xi)}\left((c + RF_2')R + A_4\right), \quad \xi \geqslant 0, \;\; R(0) = \alpha. \tag{4.2.20}$$

The constants A_2, A_3, A_4 are given by

$$A_2 = A_1 + B_1 - B_2, \quad A_3 = \frac{c}{\rho_l}(B_1 - B_2), \quad A_4 = c(B_1 - B_2 - \alpha). \tag{4.2.21}$$

We have a three-parameter family of solutions to the model Udell problem. That is, a family of solutions parameterized by A_1, B_1, B_2. These can be carefully chosen in order to have temperature increasing in both regions, and the density decreasing to the right of the interface. A typical result is shown in Fig. 10. Now we are in a position to compare numerical results with the travelling wave solution.

Note: With $B_1 < 0$ to ensure that F_1 is increasing, we have $F_1 \to -\infty$ as $\xi \to -\infty$. Clearly, the temperature in the two-phase region will become negative for some value of t, and remain negative as t increases. Our code takes the M2 comparison as $\rho_v = \min(\rho, \alpha)$. This gets around the fact that the vapour pressure becomes negative as temperature does. So, while comparison with this travelling wave solution serves the purpose of evaluating the performance of the numerical method, we note that the travelling wave solutions to this reduced problem only represent anything close to the physical problem up to the time at which T and p become negative. The solution structure of the physical problem at the interface is retained, though.

4.3. Numerical results, convergence study

In order to evaluate the performance of the M2 capturing method applied to the reduced Udell problem, we simply give our code initial conditions and boundary conditions consistent with the exact travelling wave solution given by (4.2.17)–(4.2.21), for the chosen values of the parameters A_1, B_1, B_2. In Fig. 11, we show computed interface location, noting close agreement with the exact solutions, and apparent convergence with

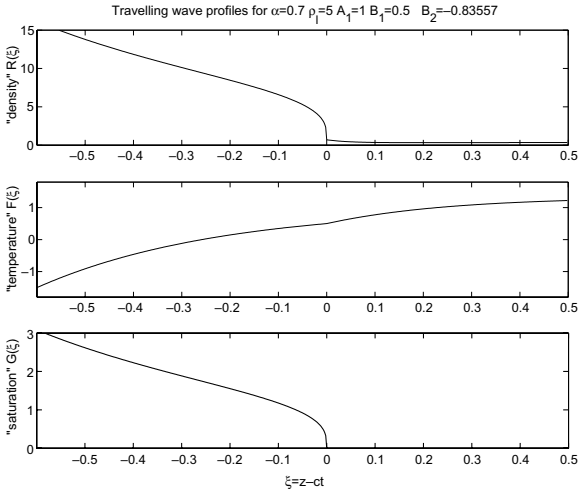

Fig. 10. Travelling wave profiles for mixture density, temperature and saturation.

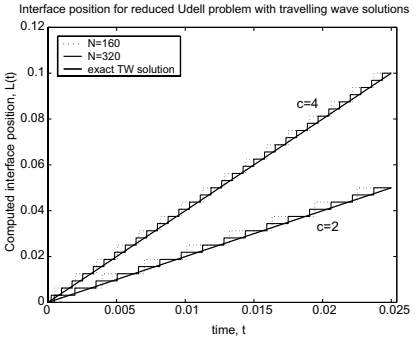

Fig. 11. Computed and exact interface location for the reduced travelling wave problem.

grid refinement. Now we will demonstrate the convergence of our schemes numerically. Although we have a second-order scheme and an exact solution, we do not expect to be able to show second-order accuracy. Firstly, we need an accurate measure of interface location. Methods are available for the enthalpy solution of the Stefan problem [22], but are based on a known phase-change temperature, and will not be applicable here. In the results shown, the interface location is simply the next grid point to the right of $s = 0$. An improved interface location would require an extrapolation from the steepening saturation profile. This is not straightforward, and has not been achieved yet.

In Tables 3 and 4, we show the results of a numerical convergence study for the finite volume, capturing method, applied to the reduced Udell problem.

We have exact solutions given by the travelling waves, with speeds $c = 1$ and 4. In both cases, we use implicit time-stepping, with $\mu = k/h^2$ fixed. We now include the error in interface location L. Specifically, we compute

$$\|E_L\|_1 = \frac{1}{\text{num}} \sum_{n=1}^{\text{num}} |L(t_n) - ct_n|.$$

Again, we see convergence at first-order. We note here that, when computing solutions to the two-phase Stefan problem with travelling wave solutions, using the enthalpy method described in [1], we found the temperature error to decrease by a factor of around 2.3 as the grid spacing is halved. Also, applying the discretization used by Evje et al., applied to the one-dimensional porous medium equation $u_t = (u^3 u_x)_x$, we found the error in

Table 3
Errors for reduced Udell problem, implicit (BE) time-stepping with $\mu = 0.2$, $c = 2$

N	num	$\|E_T\|_1$	Factor	$\|E_\rho\|_1$	Factor	$\|E_L\|_1$	Factor
20	50	1.9986 E − 3		8.1047 E − 2		1.3620 E − 2	
40	200	7.0790 E − 4	2.82	3.3881 E − 2	2.39	7.3350 E − 3	1.91
80	800	2.5842 E − 4	2.74	1.4097 E − 2	2.40	3.8450 E − 3	1.90
160	3200	9.7712 E − 5	2.64	5.8601 E − 3	2.41	2.0283 E − 3	1.89
320	12,800	3.8206 E − 5	2.56	2.4351 E − 3	2.41	1.0625 E − 3	1.91

Table 4
Errors for reduced Udell problem, implicit (BE) time-stepping with $\mu = 0.2$, $c = 1$

N	num	$\|E_T\|_1$	Factor	$\|E_\rho\|_1$	Factor	$\|E_L\|_1$	Factor
20	50	1.1646 E − 3		5.9305 E − 2		1.5220 E − 2	
40	200	3.6319 E − 4	3.21	2.6721 E − 2	2.22	7.0375 E − 3	2.16
80	800	1.2909 E − 4	2.81	1.1080 E − 2	2.41	3.7072 E − 3	1.90
160	3200	4.5586 E − 5	2.83	4.6023 E − 3	2.41	1.9445 E − 3	1.91
320	12,800	1.6463 E − 5	2.77	1.9151 E − 3	2.40	1.0119 E − 3	1.92

Table 5
Errors for Reduced Udell model, travelling wave with $c = 2$, varying time step

$\mu(= k/h^2)$	num	$\|E_T\|_1$	fac	$\|E_\rho\|_1$	fac
2	500	9.50 E − 6		1.06 E − 4	
1	1000	4.51 E − 6	2.11	5.02 E − 5	2.11
0.5	2000	2.01 E − 6	2.25	2.23 E − 5	2.25

Base solution has $N = 200$, with $\mu = 0.1, \text{num} = 10,000$.

Table 6
Errors for PME, travelling wave with $c = 1$, varying time step

$\mu(= k/h^2)$	num	$\|E_u\|_1$	fac
0.2	1000	1.55 E − 5	
0.1	2000	7.36 E − 6	2.11
0.05	4000	3.27 E − 6	2.25

Base solution has $N = 50$, with $\mu = 0.01, \text{num} = 20,000$.

u to decrease by a factor of 2.4 as the grid spacing is halved. Our capturing method for this coupled, vector, nonlinear problem clearly gives convergence rates comparable with those for these scalar prototype problems.

4.4. Temporal convergence study

As noted earlier, the computed error is dominated by the spatial error. Now we specifically demonstrate accuracy in time, by varying the time-step independently of the fixed grid size. The results shown are for the reduced model, but we use a base numerical solution with a small time-step and grid size as the exact solution, so that we concentrate on the temporal error.

In Table 5, we show a convergence study for our M2 method applied to the reduced model problem, using a travelling wave initial condition. The grid spacing is fixed as the time-step is refined. Clearly, we have first-order accuracy in time. For comparison, a similar convergence study is shown in Table 6, for the scalar Porous Medium Equation. Once again, the convergence rates for our vector problem compare very favourably with those for the much simpler scalar problem.

To conclude, we have demonstrated accuracy in both space and time for our M2 method applied to the coupled, vector Udell problem, with convergence rates comparable with those for capturing methods applied to simple prototype problems. Also, we have constructed semi-analytical solutions to a model problem, for use with further numerical and analytical studies.

5. Computations in higher dimensions

One of the distinct advantages of a fixed-domain, front-capturing method over front tracking is that extension to higher dimensions is much more straightforward. In this section, we return to the full mathematical model for the physical problem, and present some computational results in two dimensions. In particular, our point here is simply to demonstrate the robustness of our method, by choosing systems with irregular interface geometries, and those which evolve through topological changes.

5.1. Mathematical model

If we generalize the governing equations (3.1.1)–(3.1.3) to higher dimensions, we have

$$(\phi\rho_l s)_t + \nabla\cdot(\rho_l \mathbf{u}_l) = \Gamma, \tag{5.1.1}$$

where as before, u represents the Darcy velocity, and Γ is the condensation rate. Similarly, conservation of mass for the vapour phase is given by

$$(\phi\rho_{\mathrm{v}}(1-s))_t + \nabla\cdot(\rho_{\mathrm{v}}\mathbf{u}_{\mathrm{v}}) = -\Gamma. \tag{5.1.2}$$

The energy equation is now

$$(\overline{\rho c})T_t = \nabla\cdot(\widehat{K}\nabla T) + h_{\mathrm{vap}}\Gamma, \tag{5.1.3}$$

where the Darcy velocities are functions of the saturation and the vapour pressure, and are given by

$$\mathbf{u}_{\mathrm{v}} = -\frac{\kappa\kappa_{r\mathrm{v}}}{\mu_{\mathrm{v}}}\nabla p, \tag{5.1.4}$$

and

$$\mathbf{u}_{\mathrm{l}} = -\frac{\kappa\kappa_{r\mathrm{l}}}{\mu_{\mathrm{l}}}(\nabla p - \delta J'(s)\nabla s), \tag{5.1.5}$$

where μ is viscosity, κ is the permeability of the medium, $\kappa_{r\mathrm{l},r\mathrm{v}}$ are the relative permeabilities, and $J(s)$ is the Leverett function.

For our sample 2D computations, on $\Omega = (0, D)\times(0, D)$, we take periodic conditions in the x-direction. At the bottom boundary $y = 0$, take a given temperature, and no mass flux, so that

$$T = T_0(x,t), \quad (\rho_l\mathbf{u}_{\mathrm{l}} + \rho_{\mathrm{v}}\mathbf{u}_{\mathrm{v}})\cdot\mathbf{n} = 0. \tag{5.1.6}$$

At the top boundary $y = 1$, we take a higher given temperature, and no mass flux, so that

$$T = T_1(x,t)(> T_0(x,t)), \quad (\rho_{\mathrm{l}}\mathbf{u}_{\mathrm{l}} + \rho_{\mathrm{v}}\mathbf{u}_v)\cdot\mathbf{n} = 0. \tag{5.1.7}$$

Now, given that there is no mass flux across the boundary, our initial condition fixes the total water mass W.

Now, in order to compute solutions to this problem, we simply extend the finite volume scheme described in Sections 3.4 and 3.5 to the two-dimensional problem.

5.2. Computational results

The first results we show use the steady-state results for the one-dimensional problem shown in Fig. 2. The total water mass (per unit area) in the system is $W = 35.7$, and the interface is $L = 0.15$. Now, we consider the two-dimensional, transient problem with uniform boundary temperatures at $y = 0$, D corresponding to those at $z = 0$, D for the one-dimensional problem. Now we give an initial condition with a fixed water mass (per unit length) of WD. Imposing no mass flux across the lower and upper boundaries, and giving periodic conditions in x, we expect the solutions to evolve towards the one-dimensional, steady-state results shown.

In Fig. 12, we show temperature and mixture density plots at two times, for a two-dimensional initial condition which has liquid water at a uniform saturation concentrated near the lower boundary in a block as shown, and vapour in the block above it. The temperature is taken initially uniform, so that $T(x, y, 0) = T_{\mathrm{bot}} = 360$, and then the system is subject to sudden heating at $y = D$. A fully implicit scheme is used, with a 20×20 grid.

We note the evolution of the system towards the correct steady state. In Fig. 12, we can see that after a time of about 20 min, the interface is approximately at $y = 0.15$. The influence of the initial condition is still apparent, but the saturation and temperature plots have roughly the familiar shape of the steady-state one-dimensional profiles.

In Fig. 13, we plot the liquid and vapour fluxes at early and long times, on a saturation contour plot. At $t = 16$, the liquid fluxes are small everywhere except near the interface. At the later time, there is a larger liquid flux at the lower boundary, where the vapour condenses, and then is driven upwards by the capillary pressure gradient. The vapour flux in the vapour region is initially large, but decreases in time as a steady state is approached. The one-dimensional steady-state solution has stationary vapour in the vapour region. As a steady state is approached, the vapour flux becomes essentially one-dimensional.

In Fig. 14, we plot contours of saturation at increasing time, for an initial condition with a "blob" of two-phase fluid at uniform saturation in the centre of the domain. Again, we have sudden heating at the top, closed upper and lower boundaries, and periodic conditions in x. We see the two-phase region spreading, and migrating towards the lower boundary. There is initially a large downward vapour flux in the vapour region (outside

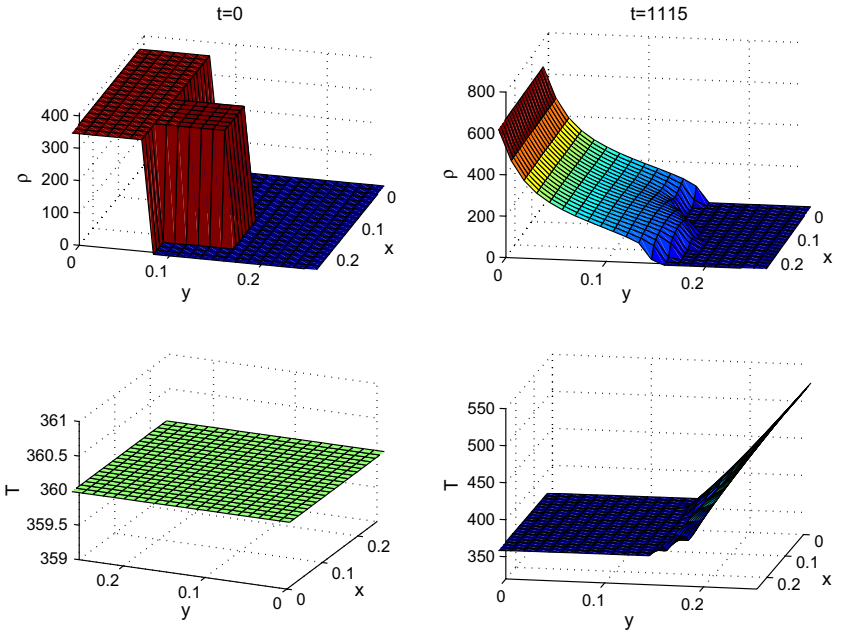

Fig. 12. Mixture density and temperature plots – initial condition and long time.

the blob), and condensation occurs at the cold boundary $y = 0$. A second two-phase region thus appears near the lower boundary, creating a second interface which is clearly visible at $t = 189$. Liquid accumulates in the lower two-phase region, and the blob migrates downwards through the surrounding vapour region, until the two separate two-phase regions coalesce, leaving just one interface once more. Our capturing method encounters no problems upon these topological changes. In this example, the total water mass in the system is equiv-

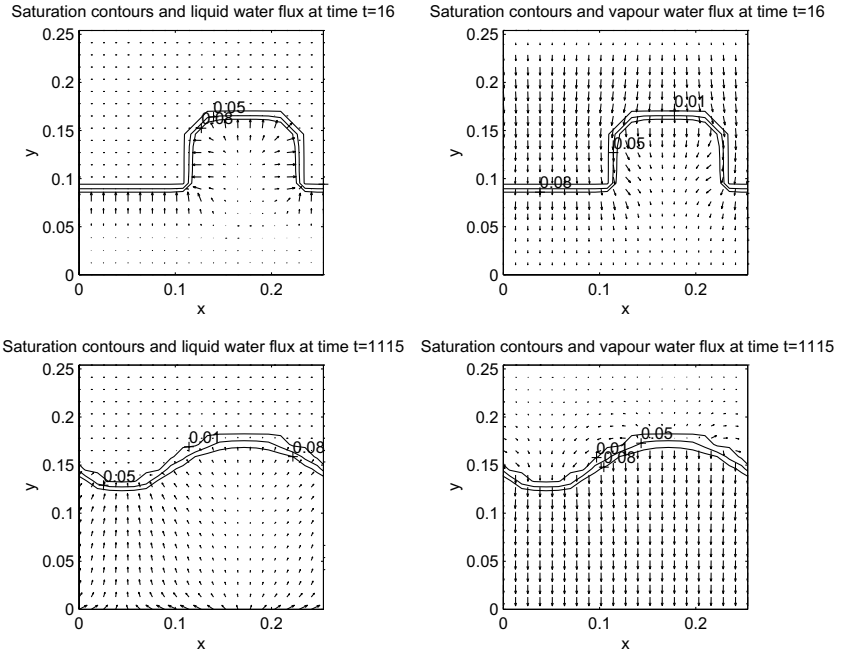

Fig. 13. Saturation contours with liquid and vapour fluxes.

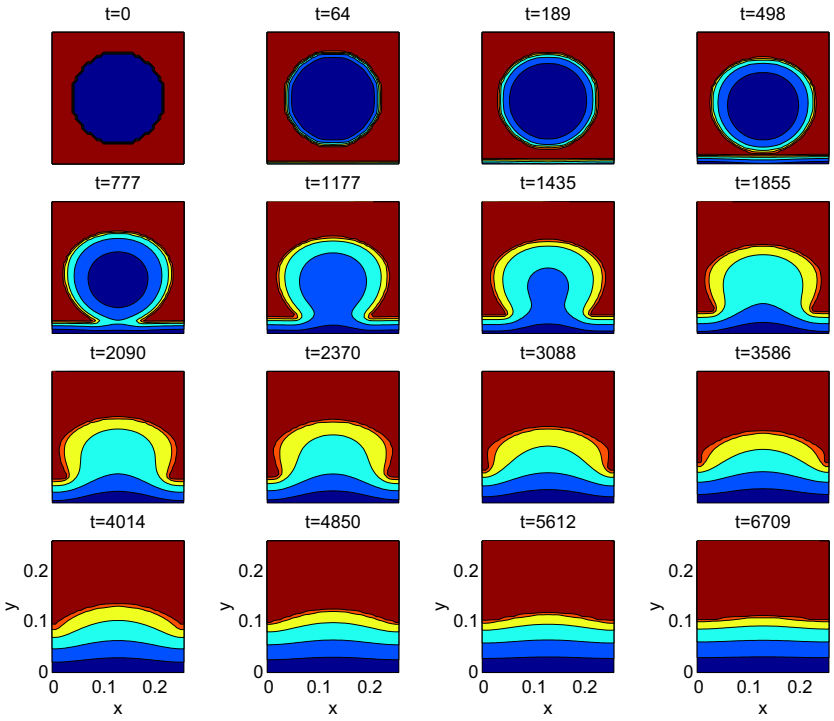

Fig. 14. Saturation contours for an initial "blob" of two-phase fluid in the centre of the domain.

alent to a one-dimensional steady-state solution with interface at $L = 0.1$. We see that, by time $t = 6709$, we have almost reached this one-dimensional steady state.

6. Conclusions and future work

In this paper, we have presented a numerical interface-capturing method for a model problem of time-dependent two-phase flow with phase change in porous media. We have allowed for a nonisothermal two-phase region, rather than making the popular assumption of an isothermal region. This will allow for computations in particular settings where thermal effects are important, such as fuel cell electrodes.

One-dimensional, steady-state results have been generated by extending an existing method to allow for compressible vapour. Our transient computations show convergence to the correct steady-state solutions, and we observe this for both one-dimensional and two-dimensional initial conditions.

We have found similarity solutions to a model vector problem for phase change in porous media. The singularity, degeneracy and coupling in the mathematical model have been retained, and we have demonstrated convergence of our numerical results to the exact travelling wave solutions, thus showing that the capturing method recovers an interface moving at the correct velocity. To our knowledge, this is the first such convergence study for a full, coupled model.

Future work will include applying this capturing method to physical and industrial problems of interest. In particular, we will look at model problems of phase change in fuel cell electrodes and oil reservoirs. Also, we will consider modified models of phase change which relax the saturation assumption which we have used in this paper.

Acknowledgments

This work was supported by MITACS in collaboration with our industrial partner Ballard Power Systems. The financial support of MITACS in the way of a student fellowship for L. Bridge is gratefully

acknowledged. We also acknowledge valuable discussions with Huaxiong Huang, Brian Seymour and Ray Spiteri.

Appendix A. The effect of a regularized "relative permeability" on the travelling wave solutions to the porous medium equation

We consider the effect of the regularization parameter η on travelling wave solutions of the Porous Medium Equation, when we replace the base equation

$$s_t = (s^3 s_z)_z, \tag{A.0.1}$$

with the regularized problem

$$u_t = ((u^3 + \eta)u_z)_z. \tag{A.0.2}$$

Here, $\eta > 0$ is some small computational parameter which smears out the interface.

Consider travelling wave solutions $s(z,t) = S(\xi), u(z,t) = U(\xi)$, where $\xi = z - ct$, and c is the wave speed. Then we have

$$-cS' = (S^3 S')', \tag{A.0.3}$$

and

$$-cU' = \left((U^3 + \eta)U'\right)'. \tag{A.0.4}$$

Eq. (A.0.3) has interface-type solutions of the form

$$S(\xi) = \begin{cases} (-3c\xi)^{1/3} & \xi < 0, \\ 0 & \xi \geqslant 0, \end{cases} \tag{A.0.5}$$

where the interface is at $\xi = 0$. Consider travelling wave profiles on $-D < \xi < \infty$, with upstream fluxes equal:

$$(U^3 + \eta)U'\big|_{\xi=-D} = S^3 S'\big|_{\xi=-D},$$

and with $U \to 0$ as $\xi \to \infty$. Then $U(\xi)$ satisfies

$$-c\xi = \frac{1}{3}U^3 + \eta \log U - \frac{\eta}{3}\log(3cD), \tag{A.0.6}$$

so the "interface" has been smeared over a region of width $\mathcal{O}(\eta)$, as shown in Fig. 15.

Now consider how the degree of smearing depends on η. We subtract (A.0.3) from (A.0.4) and integrate over $(-D, \infty)$, which gives

$$\|U - S\|_1 = (3c^{-2}D)^{1/3}\eta. \tag{A.0.7}$$

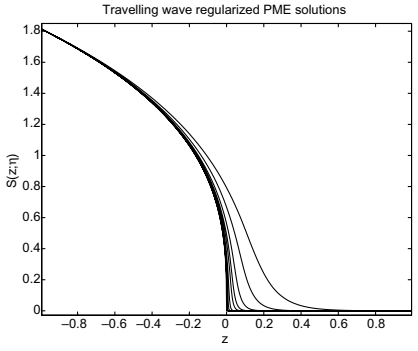

Fig. 15. Smearing of travelling wave solutions to the porous medium equation.

References

[1] V. Alexiades, A.D. Solomon, Mathematical Modeling of Melting and Freezing Processes, Hemisphere Publishing, 1993.
[2] J. Bear, Dynamics of Fluids in Porous Media, American Elsevier, 1993.
[3] R. Bradean, K. Promislow, B. Wetton, Heat and mass transfer in porous fuel cell electrodes, in: G. de Vahl Davis, E. Leonardi (Eds.), Proceedings of the International Symposium on Advances in Computational Heat Transfer Palm Cove, Queensland, Australia, May 2001, vol. 2. Begell House Inc., New York, USA, pp. 969–976.
[4] L. Bridge, Condensation in a Porous Medium, MSc Thesis, Dept. of Mathematics and Institute of Applied Mathematics, University of British Columbia, Vancouver, Canada, 2002 51pp.
[5] L. Bridge, Computational Interface Capturing Methods for Phase Change in Porous Media, PhD Thesis, Dept. of Mathematics and Institute of Applied Mathematics, University of British Columbia, Vancouver, Canada, 2006.
[6] L. Bridge, R. Bradean, M.J. Ward, B.R. Wetton, The analysis of a two-phase zone with condensation in a porous medium, J. Eng. Math. 45 (2003) 247–268.
[7] J. Crank, Free and Moving Boundary Problems, Oxford University Press, 1984.
[8] J. Divisek, J. Fuhrmann, K. Gärtner, R. Jung, Performance modeling of a direct methanol fuel cell, J. Electrochem. Soc. 150 (6) (2003) A811–A825.
[9] R.D. Donaldson, Generalised Stefan Problems – Linear Analysis and Computation, MSc Thesis, University of British Columbia, 2003.
[10] S. Evje, K.H. Karlsen, Monotone difference approximations of BV solutions to degenerate convection–diffusion equations, SIAM J. Num. Anal. 37 (6) (2000) 1838–1860.
[11] K. Hvistendahl Karlsen, K.-A. Lie, N.H. Risebro, A fast marching method for reservoir simulation, Comp. Geosci. 4 (2) (2000) 185–206.
[12] D.A. Knoll, D.B. Kothe, B. Lally, A new nonlinear solution method for phase-change problems, Num. Heat Transf., Part B 35 (1999) 439–459.
[13] M.C. Leverett, Capillary behaviour in porous solids, AIME Trans. 142 (1941) 152–169.
[14] S. Mazumder, J.V. Cole, Rigorous 3-D mathematical modeling of PEM fuel cells, J. Electrochem. Soc. 150 (11) (2003) A1510–A1517.
[15] D. Natarajan, T.V. Nguyen, A two-dimensional, two-phase, multicomponent, transient model for the cathode of a proton exchange membrane fuel cell using conventional gas distributors, J. Electrochem. Soc. 148 (12) (2001) A1324–A1335.
[16] H. Ni, A.K. Datta, K.E. Torrance, Moisture transport in intensive microwave heating of biomaterials, Int. J. Heat Mass Transf. 42 (1999) 1501–1512.
[17] J. Ockendon, S. Howison, A. Lacey, A. Movchan, Applied Partial Differential Equations, Oxford University Press, 1999.
[18] U. Pasaogullari, C.-Y. Wang, Two-phase transport and the role of micro-porous layer in polymer electrolyte fuel cells, Electrochim. Acta 49 (2004) 4359–4369.
[19] K. Promislow, J.M. Stockie, B.R. Wetton, Multiphase Transport and Condensation in a Hydrophobic PEM Fuel Cell Cathode, Preprint, June 2003.
[20] K. Pruess, C. Calore, R. Celati, Y.S. Wu, An analytical solution for heat transfer at a boiling front moving through a porous medium, Int. J. Heat Mass Transf. 30 (12) (1987) 2595–2602.
[21] K.S. Udell, Heat transfer in porous media heated from above with evaporation, condensation, and capillary effects, J. Heat Transf. 105 (1983) 485–492.
[22] V. Voller, M. Cross, An explicit numerical method to track a moving phase change front, Int. J. Heat Mass Transf. 26 (1) (1983) 147–150.
[23] C.-Y. Wang, C. Beckermann, A two-phase mixture model of liquid-gas flow and heat transfer in capillary porous media I, Int. J. Heat Mass Transf. 36 (11) (1993) 2747–2758.
[24] Z.H. Wang, C.Y. Wang, K.S. Chen, Two-phase flow and transport in the air cathode of proton exchange membrane fuel cells, J. Pow. Sources 94 (2001) 40–50.
[25] S. Whitaker, Simultaneous heat, mass and momentum transfer in porous media: a theory of drying, Adv. Heat Transf. 13 (1977) 119–203.
[26] A.W. Woods, S.D. Fitzgerald, The vaporization of a liquid front moving through a hot porous rock, J. Fluid Mech. 251 (1993) 563–579.